Seventh South African Conference on Computational and Applied Mechanics
SACAM10
Pretoria, 10−13 January 2010

NUMERICAL MODELLING OF A THIN DEFORMABLE MIRROR FOR LASER BEAM CONTROL

Craig S. Long[*,1], **Philip W. Loveday**[*,2], **Andrew Forbes**[†] **and Kevin Land**[‡]

[*]Sensor Science & Technology, CSIR Material Science & Manufacturing, Box 395, Pretoria 0001, South Africa, [1]clong@csir.co.za, [2]ploveday@csir.co.za.

[†]Mathematical Optics, CSIR National Laser Centre, Box 395, Pretoria 0001, South Africa, aforbes1@csir.co.za.
[†]School of Physics, University of KwaZulu-Natal, Private Bag X54001, Durban 4000, South Africa.

[‡]Mechatronics & Micro Manufacturing, CSIR Material Science & Manufacturing, Box 395, Pretoria 0001, South Africa, kland@csir.co.za.

Keywords: Deformable mirror, laser beam control, piezoelectric unimorph

Abstract

For intra-cavity laser beam control, a small, low-cost deformable mirror is required. This mirror can be used to correct for time-dependent phase aberrations to the laser beam, such as those caused by thermal expansion of materials. A piezoelectric unimorph design is suitable for this application. The proposed unimorph consists of a copper disc with mirror finish, bonded to a piezoelectric disc. The deformations that the mirror is required to perform are routinely (at least in optical applications) described using Zernike polynomials, which are a complete set of orthogonal functions defined on a unit disc. The challenge is to design a device that can represent selected polynomials as accurately as possible with a specified amplitude. To assist in the design process, numerical modelling is required to predict the deformation shapes that can be achieved by a unimorph mirror with a particular electrode pattern. In this paper a previously proposed axisymmetric Rayleigh-Ritz formulation, is extended to account for non-axisymmetric voltage distributions, and therefore non-axisymmetric displacements. The Rayleigh-Ritz model, which uses the Zernike polynomials directly to describe the displacements, produced a small model (stiffness matrix dimension equal to the number of polynomials used) that predicts the deformations of the piezoelectric mirror with remarkable accuracy. The results using this Rayleigh-Ritz formulation are compared to results from a traditional finite element analysis using a commercial finite element package. Both numerical models were applied to model a prototype deformable mirror and produced good agreement with experimental results.

1 Introduction

Adaptive optics is routinely used in large earth based telescopes to correct for the effects of atmospheric turbulence. These systems use large arrays of mirrors individually controlled by sets of piezoelectric stack actuators and are therefore very expensive. For intra-cavity laser beam control, a smaller, lower-cost deformable mirror is required. This mirror can be used to

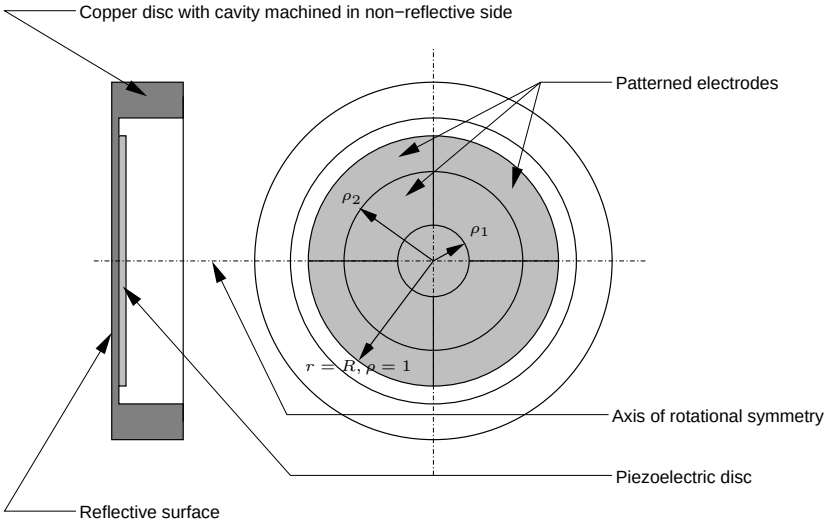

Figure 1: Side and back view of the proposed unimorph mirror design.

correct for time-dependent phase aberrations to the laser beam, such as those caused by thermal expansion of materials. A piezoelectric unimorph design, such as that depicted in Figure 1, is suitable for this application [1].

The unimorph consists of a thin copper disc with mirror finish, bonded to a piezoelectric disc. In the proposed design, the thin copper disc is formed by removing material from behind the mirror, thus leaving the disc supported by a thick and rigid rim. When a voltage is applied to the piezoelectric disc the induced strains in the plane of the disc cause bending of the unimorph. In this way relatively large displacements, compared to the 10.6 μm wavelength of the CO_2 laser, can be obtained from a small, relatively inexpensive device. The electrode on the free surface of the piezoelectric disc can be divided into numerous segments, which can each have a different voltage applied. In this way the mirror surface can be deformed into complex shapes.

In adaptive optics the imperfections in the optical system and therefore the deformations that the mirror is required to perform are described by Zernike polynomials. The Zernike polynomials form a complete set of orthogonal functions on the unit circle. The challenge is to design a device that can represent selected polynomials as accurately as possible with a specified amplitude. To this end, numerical modelling is required to predict the deformation shapes that can be achieved by a particular electrode pattern.

In this paper the axisymmetric Rayleigh-Ritz formulation, previously proposed by the authors in [2], is generalised to account for non-axisymmetric voltage (and associated displacement) distributions. The proposed Rayleigh-Ritz model has the advantage that the deformations are directly expressed in terms of the Zernike polynomials, so that no post-processing of displacements is required to interface with optical systems. The Rayleigh-Ritz model is also compact and numerically efficient. For comparison with an existing numerical model, a commercial finite element package, namely Comsol Multiphysics [3], is used. A prototype device, schematically depicted in Figure 1 was constructed and surface displacements were measured using a Polytec scanning laser vibrometer subject to various driving conditions. The results of both numerical models are then compared to the experimental measurements.

2 Zernike Polynomial Description

As mentioned previously, in optical applications aberrations, and therefore the deformations that the mirror is required to perform are routinely described using Zernike polynomials. The forms of the even and odd polynomials used in this work are, respectively given by:

$$\begin{aligned} Z_n^m(\rho,\theta) &= R_n^m(\rho)\cos(m\theta), \text{ and} \\ Z_n^{-m}(\rho,\theta) &= R_n^m(\rho)\sin(m\theta) \end{aligned} \tag{1}$$

with non-dimensionalised radius $0 \leq \rho \leq 1$; angle $0 \leq \theta \leq 2\pi$, n and m indices, and where

$$R_n^m(\rho) = \begin{cases} \sum_{k=0}^{(n-m)/2} \dfrac{(-1)^k(n-k)!}{k!((n+m)/2-k)!((n-m)/2-k)!}\rho^{n-2k} & \text{for } n-m \text{ even} \\ 0 & \text{for } n-m \text{ odd.} \end{cases} \tag{2}$$

Note that R_n^m is also only defined for $(n-m) \geq 0$. For convenience, we will use a single-index to denote the Zernike polynomials instead of the usual two-index notation presented in (1). Therefore $Z_n^m \rightarrow Z_j$, where the mode number j is given by:

$$j = \frac{n(n+2)+m}{2}. \tag{3}$$

Otherwise if the mode number is given, the radial order n and angular frequency m can be found using:

$$\begin{aligned} n &= \text{ceiling}\left(\frac{-3+\sqrt{9+8j}}{2}\right), \text{ and} \\ m &= 2j - n(n+2). \end{aligned} \tag{4}$$

The first 15 Zernike polynomials using this single-index notation are depicted in Figure 2. The Rayleigh-Ritz formulation making use of these functions to interpolate the displacements directly will now be presented.

3 Rayleigh-Ritz Model Formulation

A Rayleigh-Ritz numerical model employing Zernike polynomials directly to describe the deformation of a mirror for optical applications, was previously presented by the authors [2]. This numerical model was inspired by the work of Hagood *et al.* [4] who applied the Rayleigh-Ritz method to model a cantilever beam with attached piezoelectric ceramic patches. However, this previously developed procedure considered only axisymmetric displacements, and its scope of application is therefore limited. For example, non-axisymmetric deformations may be required to remove phase aberrations introduced as a result of manufacturing errors. Once again, Zernike polynomials will be used to directly describe the deformation of the mirror.

A generalised form of Hamilton's principle for coupled electromechanical systems is given by Hagood *et al.* [4] as:

$$\delta \int_{t_1}^{t_2} L \, \mathrm{d}t + \int_{t_1}^{t_2} \delta W \, \mathrm{d}t = 0, \quad L = T - U + W_e + W_m \tag{5}$$

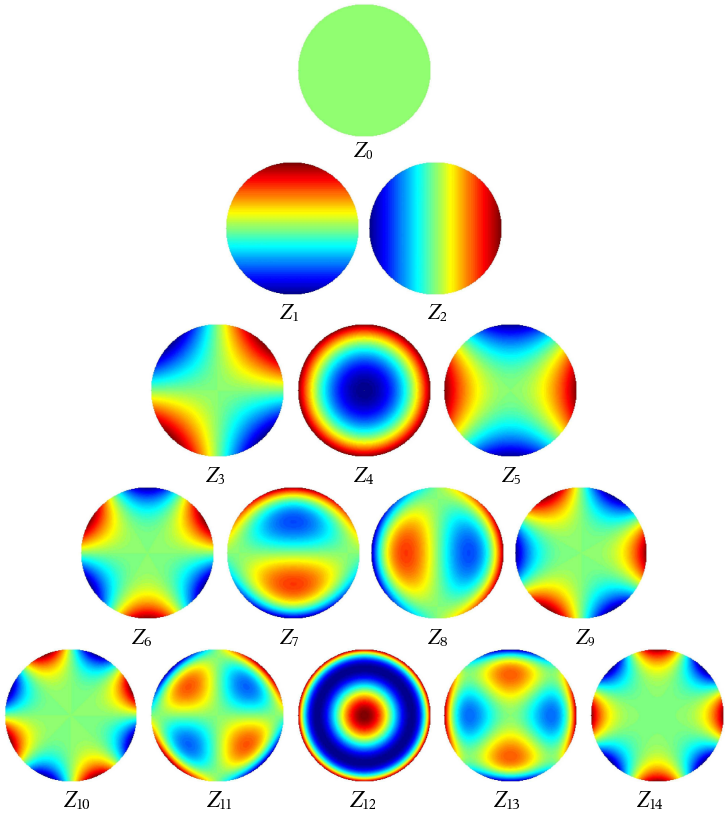

Figure 2: First fifteen Zernike polynomials labelled using a single-index notation.

in which L is the Lagrangian function and δW is the virtual work. The kinetic energy T, strain energy U, and electrical energy W_e, are respectively given by:

$$T = T_s + T_p = \int_{V_s} \frac{1}{2}\rho_s \dot{\boldsymbol{u}}^T \dot{\boldsymbol{u}} \, \mathrm{d}V + \int_{V_p} \frac{1}{2}\rho_p \dot{\boldsymbol{u}}^T \dot{\boldsymbol{u}} \, \mathrm{d}V, \tag{6}$$

$$U = U_s + U_p = \int_{V_s} \frac{1}{2}\boldsymbol{S}^T \boldsymbol{T} \mathrm{d}V + \int_{V_p} \frac{1}{2}\boldsymbol{S}^T \boldsymbol{T} \mathrm{d}V, \text{ and} \tag{7}$$

$$W_e = \int_{V_p} \frac{1}{2}\boldsymbol{E}^T \boldsymbol{D} \mathrm{d}V. \tag{8}$$

The kinetic and strain energies are decomposed into their structural i.e. non-piezoelectric and piezoelectric components, denoted by subscript s and p respectively. The effects of electrical energy, W_e, in the structure and free space due to fringing is neglected. For piezoelectric applications, the magnetic term, W_m, may be neglected. The vector of mechanical displacements is given by $\boldsymbol{u}$ and the stresses and strains by $\boldsymbol{T}$ and $\boldsymbol{S}$ respectively. The vector of electrical displacements (charge/area) is represented by $\boldsymbol{D}$ and $\boldsymbol{E}$ is the vector of the electric field in the material (volts/meter). The material density is denoted ρ.

Since our implementation is similar to that of Hagood *et al.* [4], only the details required to apply the method to the proposed geometry will be presented here. Firstly, sets of assumed displacement and electrical potential distributions are required. In this case we use the Zernike polynomials, shown in Figure 2, as the assumed displacement distributions. The normal displacement may then be written as a superposition of assumed displacement functions with

unknown coefficients as

$$w(r,\theta,t) = \boldsymbol{Z}(r,\theta)\boldsymbol{a}(t) = R\left[Z_0(\rho,\theta)\ Z_1(\rho,\theta)\ ...\ Z_n(\rho,\theta)\right]\left\{\begin{array}{c} a_0(t) \\ a_1(t) \\ \vdots \\ a_n(t) \end{array}\right\}, \tag{9}$$

where R is the radius of the disc, Z_i are the Zernike polynomials as defined in (1), $\rho = r/R$ is the non-dimensionalised radius, θ is the polar angle and $a_i(t)$ are the time dependent amplitude coefficients for the polynomials, which have to be determined. The kinematic relationships between displacements is given by

$$u = u_0 - z\frac{\partial w}{\partial r} \tag{10}$$

$$v = v_0 - \frac{z}{r}\frac{\partial w}{\partial \theta} \tag{11}$$

where u and v represent the radial and circumferential displacements respectively.

Next, a strain-displacement operator is required for the particular structure being modelled. If we limit ourselves to a thin circular plate in bending, the appropriate strain-displacement operator is given by [5] in (12), where L_w is the strain-displacement operator, w is the displacement normal to the neutral axis and z is the distance from the neutral axis, given in (9).

$$\left\{\begin{array}{c} \epsilon_r \\ \epsilon_\theta \\ \gamma_{r\theta} \end{array}\right\} = \boldsymbol{L}_w w = \left\{\begin{array}{c} \dfrac{\partial u}{\partial r} \\ \dfrac{1}{r}\dfrac{\partial v}{\partial \theta} + \dfrac{u}{r} \\ \dfrac{1}{r}\dfrac{\partial u}{\partial \theta} + r\dfrac{\partial}{\partial r}\left(\dfrac{v}{r}\right) \end{array}\right\} \tag{12}$$

The strain may then be written in terms of the unknown coefficients as

$$\boldsymbol{S}(r,\theta,t) = \boldsymbol{L}_w\boldsymbol{Z}(r,\theta)\boldsymbol{a}(t) = \boldsymbol{N}_w(r,\theta)\boldsymbol{a}(t). \tag{13}$$

It can then be shown that the resulting stiffness matrix can be written in the usual form as

$$\boldsymbol{K} = \int_V \boldsymbol{N}_w^T\boldsymbol{c}\boldsymbol{N}_w\ \mathrm{d}V, \tag{14}$$

where $\boldsymbol{c}$ is the material elastic matrix.

In a similar fashion the electrical potential field is described by assumed functions. As this is a thin piezoelectric disc it will be assumed that the electric field varies linearly through the thickness of the disc. We set the voltage on the electrode contacting the copper to be zero and the voltages on the i^{th} free electrode segment to be V_i. We assume that there is no radial or circumferential variation of the electrical potential under an electrode segment. The electrical potential under electrode segment i is therefore simply

$$V_i(z,t) = -V_i(t)(z - z_0)/h_1, \tag{15}$$

where z_0 is the position of the neutral axis and h_1 is the thickness of the piezoelectric ceramic. The electric field is simply the negative of the gradient of the voltage ie., $\boldsymbol{E}(t) = V_i(t)/h_1$, and the complete field is written as,

$$\boldsymbol{E}(t) = [1/h_1 \; 1/h_1 \; ... \; 1/h_1] \left\{ \begin{array}{c} V_1(t) \\ \vdots \\ V_m(t) \end{array} \right\} = \boldsymbol{N}_v \boldsymbol{V}(t). \tag{16}$$

The piezoelectric coupling matrix is then,

$$\boldsymbol{\vartheta} = \int_V \boldsymbol{N}_v^T \boldsymbol{e} \boldsymbol{N}_w \, \mathrm{d}V, . \tag{17}$$

where $\boldsymbol{e}$ is the piezoelectric coupling material matrix. The mass matrix $\boldsymbol{M}$ and capacitance matrix $\boldsymbol{C}_p$ can be implemented if we wish to compute natural frequencies, as follows:

$$\boldsymbol{M} = \int_V \boldsymbol{Z}^T \rho \boldsymbol{Z} \, \mathrm{d}V, \text{ and} \tag{18}$$

$$\boldsymbol{C}_p = \int_V \boldsymbol{N}_v^T \boldsymbol{\epsilon} \boldsymbol{N}_v \, \mathrm{d}V, \tag{19}$$

where $\boldsymbol{\epsilon}$ is the material capacitance matrix. The coupled electromechanical equations are then,

$$\begin{aligned} \boldsymbol{K}\boldsymbol{a} - \boldsymbol{\vartheta}\boldsymbol{V} &= \boldsymbol{F} \\ \boldsymbol{\vartheta}^T \boldsymbol{a} + \boldsymbol{C}_p \boldsymbol{V} &= \boldsymbol{Q}, \end{aligned} \tag{20}$$

where $\boldsymbol{F}$ and $\boldsymbol{Q}$ represent the applied forces and charges respectively. The procedure proposed in [2] to compute the material properties ($\boldsymbol{c}$, $\boldsymbol{e}$ and $\boldsymbol{\epsilon}$) for a thin piezoelectric disc, is again used here. Similarly, the process to compute the $z-$position of the neutral axis (z_0), by minimizing the strain energy or flexural rigidity, proposed in [2] is employed. The integrals required to construct (20) can conveniently be computed *analytically* using symbolic mathematics software such as Mathematica or Maxima.

Since the proposed mirror design has a thin deformable membrane spanning a thick and relatively rigid rim, some special attention has to be paid to the boundary conditions. In particular, the Lagrangian presented in (5) is modified as follows:

$$\tilde{L} = L + \frac{1}{2} k_r \cdot [w(r = R)]^2 \tag{21}$$

where k_r is a parameter related to the stiffness of the rim, and where $w(r = R)$ is the displacement at the outer radius of the disc $r = R$. As $k_r \to \infty$, $w(r = R) \to 0$ simulating a completely rigid rim. However, realistic values for k_r could also be estimated using plate theory to simulate a flexible attachment if necessary.

4 Experimental Details

In order to assess the practicality of the proposed numerical models, a physical prototype of the device depicted in Figure 1 was constructed. The prototype unimorph-type deformable mirror consists of a 40 mm diameter, 0.3 mm thick, PZT4 piezoelectric ceramic disc bonded to

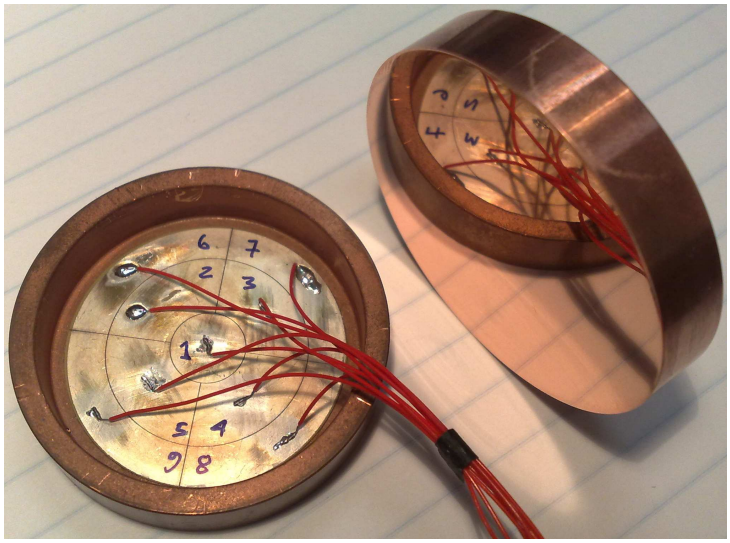

Figure 3: Photograph of mirror prototype showing electrode pattern.

a copper disc 44 mm in diameter and 0.3 mm thick. The copper disc is formed by machining material from behind the reflective surface until the membrane is formed, spanning the rigid rim. The free electrode on the piezoelectric disc is segmented into nine separate electrodes (three concentric rings and then the two outer rings are further divided into four segments each) as shown in Figure 3. The electrode patterning was carried out using laser ablation with an excimer laser. The unimorph was driven by applying a harmonic voltage excitation to the segmented electrodes. Point deformations on the mirror surface were measured using a Polytec scanning laser vibrometer.

In order to interface with optical systems, and to compare the experimental (as well as the conventional finite element analysis) results with the Rayleigh-Ritz model, a procedure is required to determine which of the Zernike polynomials are excited. To this end, a least-squares fit of the surface displacements is employed, i.e. we minimize the function

$$\chi^2 = \sum_{i=1}^{N} \left[y_i - \sum_{k=0}^{M} a_k Z_k(r_i, \theta_i) \right]^2 , \tag{22}$$

where y_i is the i^{th} of the N surface nodal displacements. The minimization is carried out using the procedure described in [1]. The output of this process is a vector of the coefficients a_k which scale the magnitude of the M Zernike polynomials Z.

5 Comparison of Results

In this section, the two numerical models are compared to experimental results. Firstly, the actual displacements will be compared qualitatively, after which the extracted Zernike polynomials will be compared quantitatively. The Rayleigh-Ritz model employed in the comparison makes use of 66 interpolation terms in total (Z_0, Z_1, ... Z_{65}, or up to 10^{th} radial order). The same number of polynomials were therefore also extracted from the finite element analysis and the experimental results.

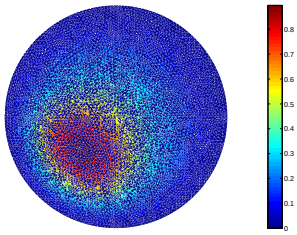

(a) Computed surface deformation (Comsol Multiphysics).

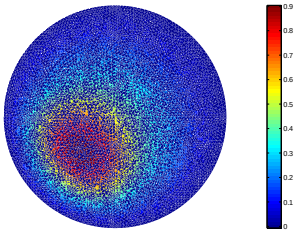

(b) Fitted surface deformation (Comsol Multiphysics).

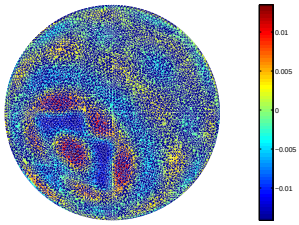

(c) Difference between computed and fitted (Comsol Multiphysics).

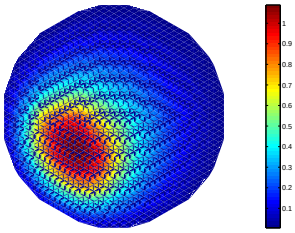

(d) Measured surface deformation (experiment).

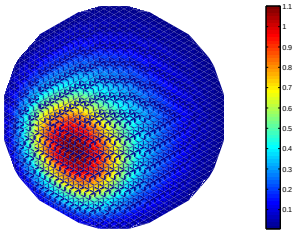

(e) Fitted surface deformation (experiment).

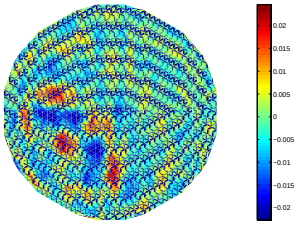

(f) Difference between measured and fitted (experiment).

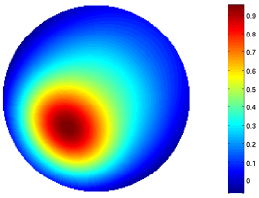

(g) Computed surface deformation (Rayleigh-Ritz).

Figure 4: Computed, measured and fitted displacements driving electrode 4 (see Figure 3) at 20 V and with all other electrodes grounded. Displacements in μm.

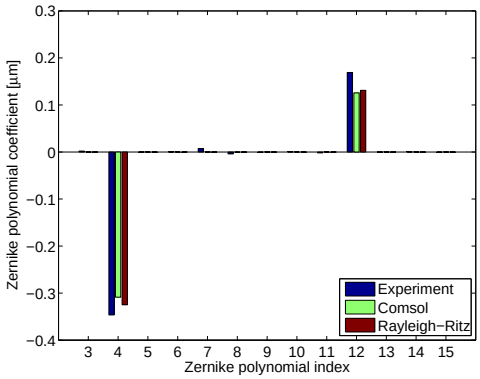

(a) First thirteen non-rigid body Zernike polynomial coefficients (Z_3 to Z_{15}).

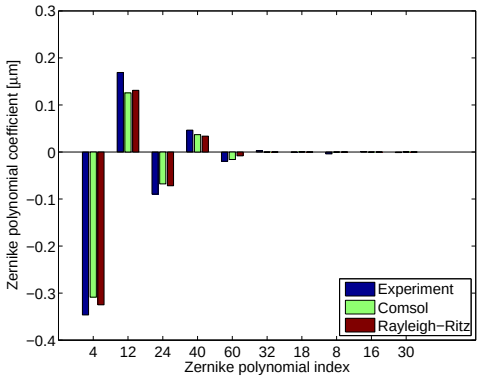

(b) Ten largest Zernike polynomial coefficients.

Figure 5: Comparison of extracted and computed Zernike polynomials resulting from application of a driving voltage of 20 V applied to electrode 1 (see Figure 3) with all other electrodes grounded.

For the qualitative comparison between measured and numerical mirror deformations, a non-axisymmetric voltage distribution is selected. The prototype mirror is arbitrarily excited by applying a voltage of 20 V to electrode 4 (see Figure 3) with all other electrodes grounded. The elastic modulus of copper was set to E=110 GPa and a Poisson's ratio of $\nu = 0.33$ was used. The required material properties used for the piezoelectric material in both numerical models were as follows:

$$s_{11}^E = 12.3 \times 10^{-12}\ \text{m}^2/\text{N}; \quad s_{12}^E = -4.05 \times 10^{-12}\ \text{m}^2/\text{N}; \quad s_{66}^E = 32.7e \times 10^{-12}\ \text{m}^2/\text{N};$$

$$d_{31} = -123 \times 10^{-12}\ \text{m/V}; \quad \epsilon_{33}^E = 635 \times 8.85 \times 10^{-12}\text{F/m}.$$

As in [2], the extent of the first electrode is from $\rho = 0$ to ρ_1, the second ring of four electrodes is from $\rho = \rho_1$ to ρ_2, and the third from $\rho = \rho_2$ to 1. The electrodes were positioned where they would be expected to best excite the third Zernike polynomial, i.e. $\rho_1 = 0.27$ and $\rho_2 = 0.72$. These points are found in [2].

Figure 4 depicts the displacements computed using the two numerical models (Figures 4(a) and 4(g)) together with the measured displacements (Figure 4(d)). Also plotted in Figures 4(b) and 4(e) are the displacements fitted to the finite element and experimental results respectively, using the extracted Zernike polynomial coefficients. The fitting errors are also depicted in Figures 4(c) and 4(f) for the Comsol Multiphysics and experimental results respectively.

Figure 4 demonstrates that the results of both numerical models and the experimental result are qualitatively similar in shape. The values of the maximum displacements are also very similar, with the experimental displacements slightly higher than the results of the two numerical models. This suggests that attention should be paid to the material properties in future works. The figure also demonstrates that the fitting procedure was correctly implemented.

In order to quantitatively compare the predicted and measured results, the coefficients of the Zernike polynomials computed using the proposed Rayleigh-Ritz method are compared to those extracted from the Comsol Multiphysics model and the experimental measurements. Figure 5 depicts the results for the axisymmetric case where the centre electrode (electrode 1 in

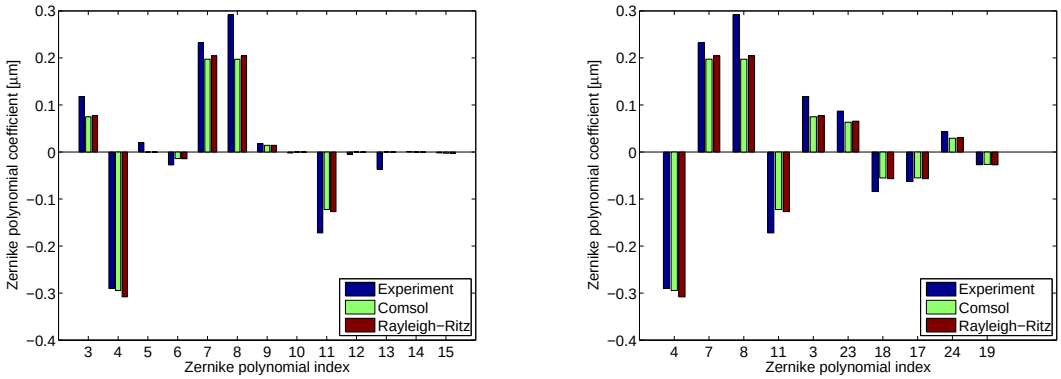

(a) First thirteen non-rigid body Zernike polynomial coefficients (Z_3 to Z_{15}).

(b) Ten largest Zernike polynomial coefficients.

Figure 6: Comparison of extracted and computed Zernike polynomials resulting from application of a driving voltage of 20 V applied to electrode 4 (see Figure 3) with all other electrodes grounded.

Figure 3) is driven with 20 V and all other electrodes are grounded. Figure 5(a) depicts the coefficient of the first thirteen non-rigid body Zernike polynomial coefficients, i.e. a_3 to a_{15} corresponding to Z_3 to Z_{15}). In Figure 5(b), the coefficients are sorted and the ten largest non-rigid body coefficients are plotted.

From Figure 5(b) it is clear that only the axisymmetric Zernike polynomials are excited, with Z_4, Z_{12}, Z_{24}, Z_{40} and Z_{60} all being axisymmetric modes. As expected, the magnitude of the coefficients decays from low orders of Zernike polynomials to higher orders. Good agreement between the two numerical models is achieved. The extracted coefficients also agree well with axisymmetric models previously developed by the authors [2].

In order to further verify the implementation, the coefficients extracted from the previously studied non-axisymmetric case depicted in Figure 4 are quantitatively compared in Figure 6. In particular, Figure 6 depicts the results for the non-axisymmetric case where electrode 4 in Figure 3 is driven with 20 V all other electrodes are grounded. Once again, Figure 6(a) depicts the coefficient of the first thirteen non-rigid body Zernike polynomial coefficients and Figure 6(b) the coefficients of the ten largest non-rigid body coefficients. Once again, excellent agreement between the numerical results is achieved, as well as good agreement with experimental results.

6 Conclusion and Planned Future Work

In this paper, a previously proposed axisymmetric Rayleigh-Ritz model was extended to account for non-axisymmetric displacements. The method proposed produces a small model (stiffness matrix dimension equal to the number of polynomials used) that predicts the deformations of the unimorph-type deformable mirror with remarkable accuracy. This method also provides insight into the operation of the device and can be used in future to optimize the design in an elegant manner since the parameters of the design are analytically available. Excellent agreement between the proposed Rayleigh-Ritz model and the Comsol Multiphysics model was achieved. The conventional Comsol Multiphysics model, however naturally requires significantly more computational effort. The results from the proposed Rayleigh-Ritz model would

therefore provide a good starting point for more detailed finite element modelling.

Future work planned for this effort will focus on the practical construction of a more refined deformable mirror. In order to used such a mirror in a laser, specification on the initial flatness of the mirror are extremely tight (usually in the order of $\lambda/20$, in the case of the CO_2 laser considered here $\lambda = 10.6\ \mu$m). Currently facilities in South Africa do not exist to manufacture a thin copper mirror to these specifications. In order to achieve this flatness, it will be attempted to spin-coat PDMS onto the copper mirror to achieve an optically flat surface. Since PDMS is not reflective, a gold coating will be deposited to achieve the desired reflectivity. Work in this direction has already been started and good reflectivity from the gold coating has been achieved at low laser power density.

References

[1] E.M. Ellis. *Low-cost bimorph mirrors in adaptive optics*. PhD thesis, Imperial College of Science, Technology and Medicine, University of London, 1999.

[2] P.W. Loveday, C.S. Long, A. Forbes, and K. Land. Modelling and optimization of a deformable mirror for laser beam control. In *Proc. 6th South African Conference on Computational and Applied Mechanics (SACAM08)*, Cape Town, South Africa, March 2008. Paper no. 21.

[3] Comsol Multiphysics (http://www.comsol.com/).

[4] N.W. Hagood, W. Chung, and A. von Flotow. Modeling of piezoelectric actuator dynamics for active structural control. *Journal of Intelligent Material Systems and Structures*, 1(3):327–354, 1990.

[5] A. Leissa. *Vibration of plates*. Acoustical Society of America, 1993.